International Conference on Green Technology and Sustainable Development
September 29-30, 2012, Hochiminh City, Vietnam

DESIGN OF AN ULTRASONIC STEEL HORN WITH A BÉZIER PROFILE

Hai-Dang Tam Nguyen, Dung-An Wang*

Graduate Institute of Precision Engineering, National Chung Hsing University, Taichung 40227, Taiwan, ROC
*** Corresponding author. Tel: +86 422840531 ext 365, Fax: +86 422858362,**
E-mail: daw@dragon.nchu.edu.tw

ABSTRACT

A novel ultrasonic steel horn with a Bézier profile is developed. The first longitudinal displacement mode of the horn is exploited for high displacement amplification. An optimization scheme and finite element analyses are used to design the horn. The displacement amplification and stress distribution characteristics of the Bézier horn and catenoidal horn are examined. Prototypes of the horns are manufactured by a laser cutting process. Performances of the proposed horn are evaluated by experiments. Experimental results of the harmonic response of the fabricated horn confirm the effectiveness of the design method. The displacement amplification of the proposed horn is 62% higher than that of the traditional catenoidal horn with the same length and end surface widths.

INTRODUCTION

Ultrasonic horns have been widely used in atomizers [1], ophthalmic surgery [2], welding devices [3], wire bonding [4,5], ultrasonic motor [6], ultrasonic lubrication [7] and ultrasonic bistoury [8], etc. Ultrasonic horn of different profiles such as Gaussian [9], Fourier, exponential [10], stepped [11,12], sinusoidal [13], conical, catenoidal [14] and spline [15], have been proposed and investigated by many researchers. Salmon [16] synthesized a horn where the profile is a perturbation from the exponential contour. In comparing with the traditional horns, new horns with non-straight structures may offer higher displacement amplification. Sherrit et al. [17] presented a folded horn in order to reduce the length of the resonator. Iula et al. [17] proposed an ultrasonic horn vibrating in a flexural mode.

Conical, exponential, catenoidal, stepped and Gaussian are the most commonly used horns [18]. Abromov [18] points out that the displacement amplification of catenoidal horns is greater than that of exponential or conical ones and less than that of stepped horns. Gaussian horns may possess high displacement amplification, but numerical methods might be needed for the design of Gaussian horns.

Parametric curve based geometry is flexible enough to give a much better control over the profile of horns for design purpose. In parametric form each coordinate of a point on a curve is represented as a function of a single parameter [19]. Therefore, it has more potential to find higher displacement amplification while keeping the stress in the horns low. Because the parametric curve has more freedom to define the horn profile, it is a more difficult problem to optimize the performance of the horn. Finite element method (FEM) has been used to study and analyze behaviors of horns [17,20]. Using FEM, detailed stress and displacement distributions can be obtained. Fu et al. [21] discussed the design of a piezoelectric transducer with a stepped horn via multiobjective optimization. They formulated the optimization problem using Pareto-based multiobjective genetic algorithms [21]. In order to design horns with conflicting design objectives, the genetic algorithms capable of finding multiple optimal solutions in a single optimization run may be used.

In this investigation, design and analysis of a steel horn for high displacement amplification are presented. The design is based on a cubic Bézier curve. The optimal designs of the horns are sought by a multiobjective optimization algorithm. Prototypes of horns are fabricated and tested. The experimental results are in good agreement with those based on the optimization design procedure.

DESIGN

Fig. 1 schematically shows a horn driven by a Langevin transducer. The horn is a displacement amplifier designed to work in a longitudinal mode. The Langevin transducer is composed of a couple of piezoelectric disks poled along *y* direction but with opposite polarities. The flange allows the mounting of the Langevin transducer at the longitudinal nodes. The horn is actuated by the transducer at the designated frequency, which is set to be the working frequency, 28.0 kHz, of the Langevin transducer used in the experiment. The nearly uniformly distributed displacement of the Langevin transducer is transformed into a longitudinal deformation of the horn. A typical displacement distribution curve is

also shown in the figure. By proper design of the horn structure, the longitudinal mode of vibration of the horn can be excited, and a large displacement amplification can be obtained.

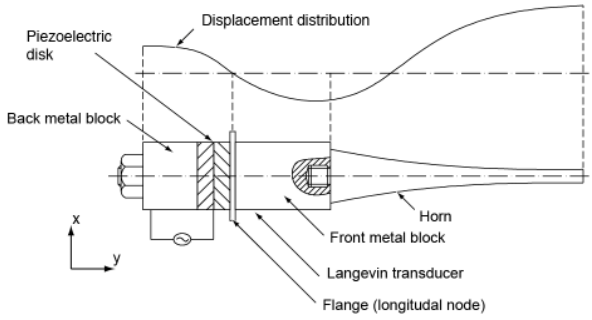

Fig. 1. Schematic of a horn and a Langevin transducer.

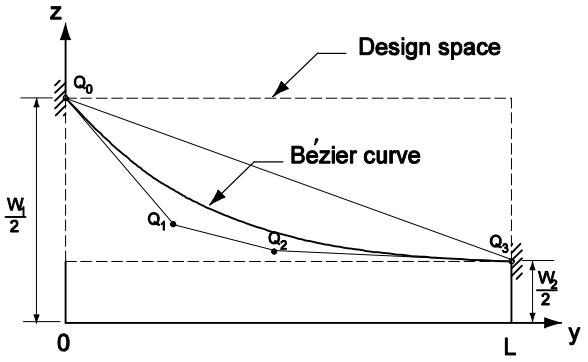

Fig. 2. A profile of a Bézier horn and its four control points Q_0 Q_1 Q_2 Q_3.

The design of the horn for high displacement magnification is based on an optimization procedure where the profile of the horn is optimized via the parameters of a cubic Bézier curve to meet the requirement of displacement amplification. The cubic Bézier curve is determined by a four-point Bézier polygon Q_0 Q_1 Q_2 Q_3 as shown in Fig. 2.

As described by Rogers and Adams [19], the first and last points, Q_0 and Q_3, respectively, on the curve are coincident with the first and last points of the defining polygon. The tangent vectors at the ends of the curve have the same directions as the first and last polygon spans, respectively. The parametric cubic Bézier curve is given by [19]

$$P(t) = \begin{bmatrix}(1-t)^3 & 3t(1-t)^2 & 3t^2(1-t) & t^3\end{bmatrix} \begin{bmatrix} P_{Q_0} \\ P_{Q_1} \\ P_{Q_2} \\ P_{Q_3} \end{bmatrix} \quad 0 \le t \le 1 \tag{1}$$

where t is the parameter, and P_{Q_i} is the position vector of the point Q_i.

The profile of the horn is optimized by allowing points Q_1 and Q_2 to move in the design space enclosed by the dashed rectangle in Fig. 2. The positions of the points Q_0 and Q_3 are fixed by the specified widths of the back and front end of the horn, W_1 and W_2, respectively, and the length of the horn, L. The horn has a specified thickness of 1.2 mm. An optimization procedure is developed and outlined in Fig. 3. The non-dominated sorting genetic algorithm [22] is applied to the optimization of the horn profile. The algorithm is suitable for solving constrained multiobjective problems. The genetic algorithm uses a binary tournament selection and the crowded-comparison operator [22]. In the binary tournament selection process, two individuals are selected at random and their fitness is compared. The individual with better fitness is selected as a parent. The crowded-comparison operator guides the selection process at the various stages of the algorithm toward a uniformly spread-out Pareto-optimal front [22].

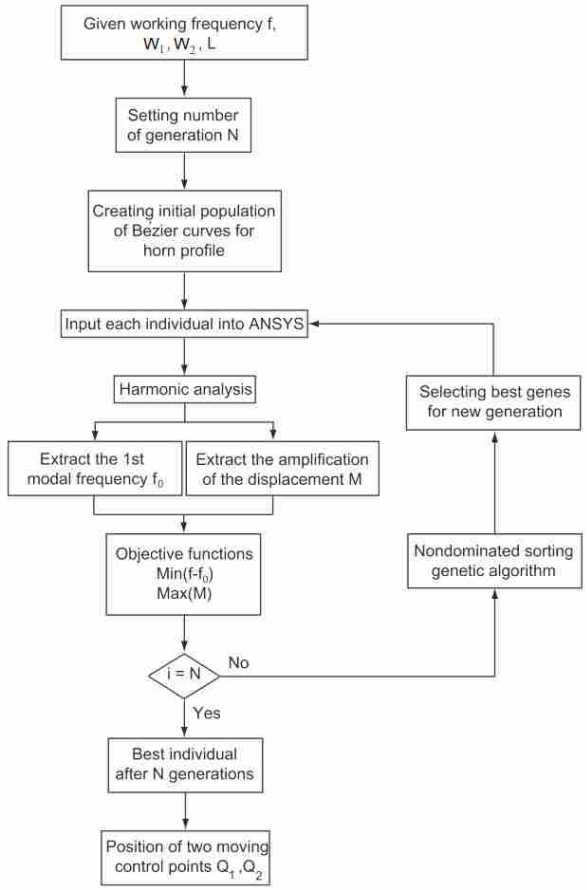

Fig. 3. Flowchart of the optimization procedure.

In the optimization process as shown in Fig. 3, initially, the working frequency f and the geometry parameters W_1, W_2 and L are specified. The objective functions of the optimization problem are

$$\begin{aligned} &Min \quad f - f_0 \\ &Max \quad M = \frac{u_{Q_3}}{u_{Q_0}} \end{aligned} \tag{2}$$

where f_0 is the first longitudinal modal frequency of the population of each generation of the horn. M is the amplification of the displacement defined by the ratio of the longitudinal displacement at the front end to that of the back end of the horn. The fast

nondominated sorting approach [22] is used to solve the two-objective optimization problem. In the sorting procedure, the concept of Pareto dominance [23] is utilized to evaluate fitness or assigning selection probability to solutions. The population is classified into non-dominated fronts based on its rank in the population, not its actual objective function values.

The proposed horn is designed to have the same working frequency as the Langevin transducer. Due to the geometry complexity, the modal frequency f_0 and the displacement amplification M of the Bézier horn cannot be calculated analytically. Finite element analysis by a commercial software ANSYS is utilized to obtain f_0 and M of the horn. The genetic algorithm optimization procedure used in this investigation is programmed with the commercial software MATLAB 7.0. The genetic algorithm, the design parameters (the four control points Q_i of the Bézier curve) and the geometry constraints are written in a script file of MATLAB. The profile of the horn is calculated and the coordinates of all nodes along the profile is created in the script file. An ANSYS text file for the harmonic analysis to obtain the modal frequency f_0 and the displacement amplification M is created by the MATLAB file. The output of the ANSYS harmonic simulation is saved in a text file. The first longitudinal modal frequency and the displacement distribution along the horn can be found in the file, and are used as the objective functions for the optimization process.

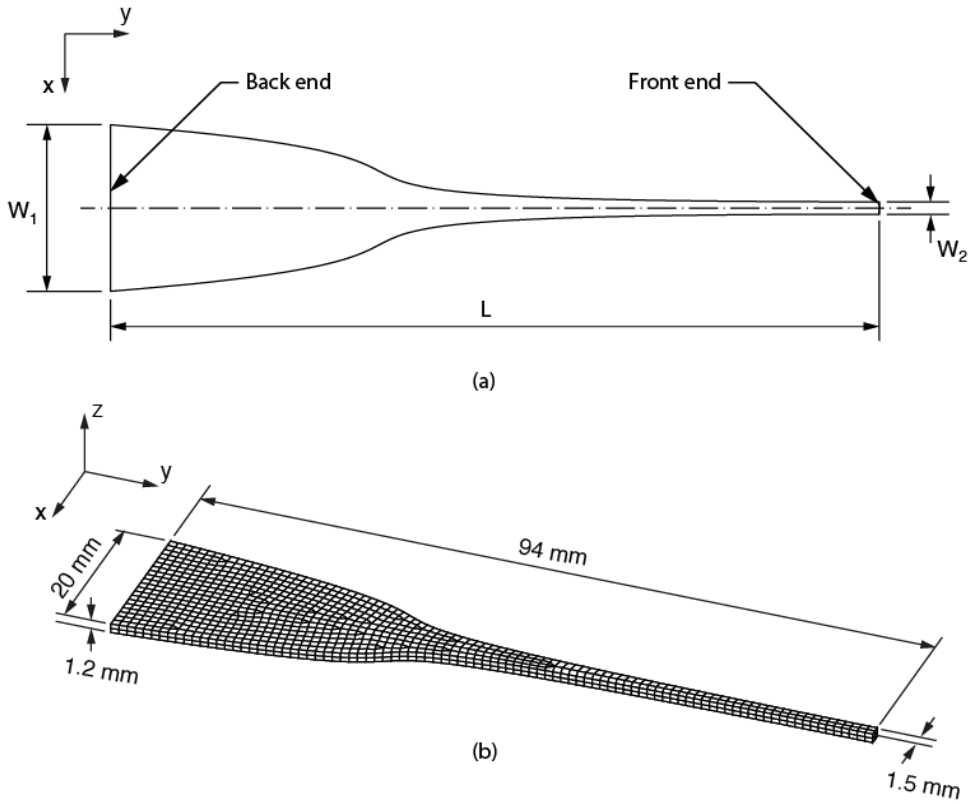

Fig. 4. (a) Schematic of the horn with the length L and the widths W_1 and W_2 of the back and front ends. (b) A mesh for an axisymmetric finite element model.

ANALYSES

Finite element model

In order to obtain accurate modal frequency and displacement solutions for the proposed horn, finite element analyses are carried out. Fig. 4(a) shows a schematic of the horn with the length L and the widths W_1 and W_2 of the back and front ends, respectively. A Cartesian coordinate system is also shown in the figure. Fig. 4(b) shows a mesh for a finite element model. A harmonic displacement in the y direction is applied to the nodes at the back end surface of the horn. In this investigation, the material of the horn is assumed to be linearly elastic. The Young's modulus and Poisson's ratio are taken as 210 GPa and 0.3, respectively. The density is taken as 7800 Kg/m^3. The commercial finite element programs ANSYS and Abaqus are employed to perform the computations. Two-dimesional 8-node quadratic element PLANE183 and 20-node quadratic brick C3D20 are used to model the horn.

Numerical analysis

In the optimization process, the number of generations, N, is set to be 50, and the population of each generation is taken as 20. In the analyses, we have also set N = 60, 70, 80, 90 and 100. However, there is no improvement with N greater than 50. The

length L and the widths W_1 and W_2 of the back and front end of the horn are specified as 94 mm, 20 mm and 1.5 mm, respectively. The working frequency f is set to be 28.0 kHz. In the experiments, the fabricated horn is driven by a Langevin transducer. The available commercial Langevin transducer is purchased from a local vendor. The working frequency of the Langevin transducer is a known and fixed parameter. The Bézier horn is designed to have its first modal frequency equal to the working frequency of the transducer. Therefore, we only consider the horn in the optimization process. Indeed, the modal frequency of the structure including transducer, flange and the horn should be different from that of the horn alone. In this investigation, we concentrate on the design of the new horn. In order to obtain better performance of the horn, its working frequency should be taken as the modal frequency of the whole structure including its driving unit and the flange.

A modal analysis in ANSYS of each population is performed in order to find its first modal frequency f_0 and displacement amplification M. Fig. 5 shows the distribution of the population of several generations in the optimization process. The abscissa represents the difference between f and f_0. The ordinate represents the displacement amplification. The displacement amplification is increased dramatically after 50 generations. As also shown in Fig. 5, the difference between f and f_0 of the best population in the last generation is zero.

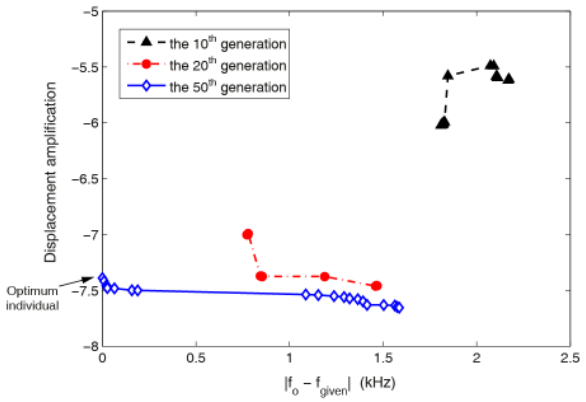

Fig. 5. Distribution of the population of several generations in the optimization process.

Based on the finite element analyses by using the commercial software Abaqus, a typical normalized frequency response function (FRF) of the model of the best population is shown in Fig. 6. In the frequency range of 0–50 kHz, the front end of the horn has its maximum displacement at 28.2 kHz.

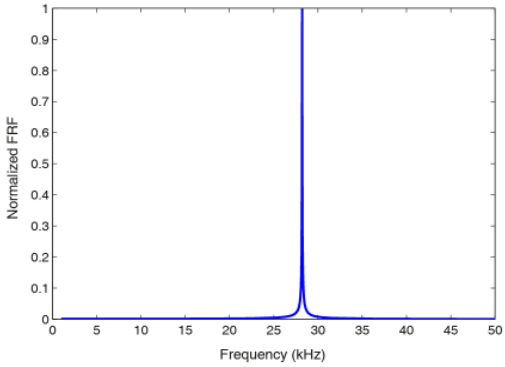

Fig. 6. A typical normalized frequency response function of the model.

A large number of modes should be responsive when the horn is excited longitudinally in the frequency range of 0–50 kHz, but Fig. 6 only illustrates one longitudinal mode since the responses of many modes are small compared to this longitudinal mode. In order to characterize the intermodal responses, the mode combinations for possible combination resonance are considered. Three of the mode shapes are shown in Fig. 7. The whole system modes involve contributions from the horn and the transducer. These modes, corresponding to a bending mode (Fig. 7(a)), a radial expansion mode (Fig. 7(b)), and a longitudinal mode (Fig. 7(c)), occur at 10,777 Hz (ω_2), 17,454 Hz (ω_3) and 28,208 Hz (ω_1), respectively, and satisfy the combination resonance, $\omega_1 \cong \omega_2 + \omega_3$. When the system is excited close to its first longitudinal mode, the internal modes, excited through the combination resonance, are excited at a much smaller response levels as seen in Fig. 6. It is assumed that modal interactions may not occur. This assumption is verified by the experimental measurements of the flexural displacement of the horn when the horn is driven longitudinally in the frequency range of 0–50 kHz.

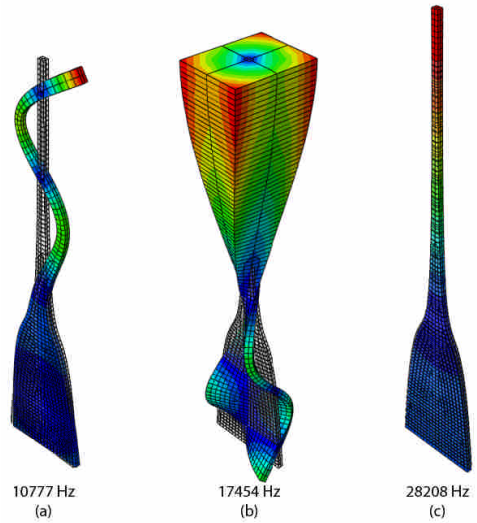

Fig. 7. The internal modes determined by finite element analyses.

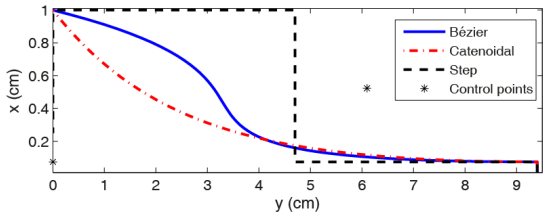

Fig. 8. Profiles of the horns.

Fig. 8 shows the profile of an optimized Bézier horn. The position of its control points are also shown in the figure. In order to compare the performances of the proposed horn with classical horns, a catenoidal horn and a stepped horn are also modeled. The stepped horn has the largest displacement amplification among the commonly used horns. However, its high stress occurring near the abruptly changing section is not favoured. The catenoidal horn has smaller displacement amplification and a smoother stress distribution than the stepped horn. The new horn discussed in this paper may have larger displacement amplification than the catenoidal horn, and lower stress concentration than the stepped horn. Here, the stepped, catenoidal and Bézier horns are selected based on the criteria of displacement amplification and Mises stress.

For fair comparison, the catenoidal horn has the same back and front end widths and length as those of the proposed horn. The working frequency of the catenoidal horn obtained by a finite element analysis is 27.8 kHz. The back and front end widths of the stepped horn are the same as those of the proposed horn. The working frequency of the stepped horn obtained by a finite element analysis is 26.7 kHz. The profiles of the catenoidal and stepped horns are also shown in Fig. 8.

Fig. 9 is a plot of the normalized displacements along the normalized length of the horns based on finite element computations. The displacements are normalized by the displacement at the back end of the horns. Therefore, the normalized displacement at the normalized length of 1 represents the displacement amplification. The stepped horn has the largest displacement amplification among the three types of the horns. The displacement amplification of the Bézier horn is much larger than that of the catenoidal horn.

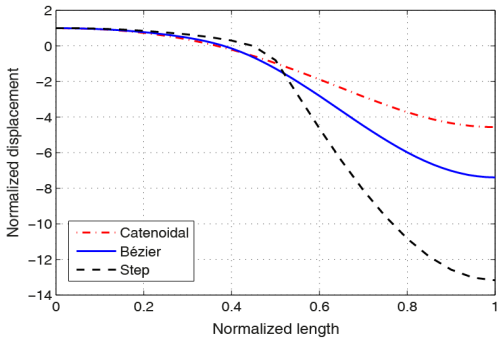

Fig. 9. Normalized displacements along the normalized length of the horns.

Fig. 10 shows the Mises stress along the normalized length of the horns based on the finite element computations. For the stepped horn, high stress occurs near the abruptly changing section. Stress concentration of the Bézier horn is significantly less than the other two types of horns. The lower Mises stress of the proposed horn can be attributed to its bell-shaped profile. The values of the displacement amplification M and maximum Mises stress σ_{max} of the three types of the horns are listed in Table 1. Although the stepped horn gives the highest displacement amplification, its high stress concentration at the step discontinuity makes it prone to failure.

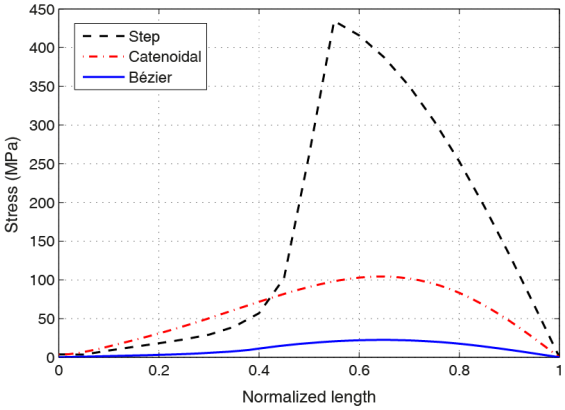

Fig. 10. von Mises stress along the normalized length of the horns.

Table 1. Comparison of the three types of the horns

	W_1/W_2	Length (mm)	*M*	σ_{max} (MPa)
Catenoidal	13.3	94	4.56	104.3
Stepped	13.3	94	13.18	434.4
Bézier	13.3	94	7.39	22.4

EXPERIMENTS AND DISCUSSIONS

In order to verify the effectiveness of the proposed horn, prototypes of a Bézier horn and a catenoidal horn are fabricated by a laser cutting process from a stainless steel. Dimensions of the prototypes are based on the finite element analyses. Fig. 11 is a photo of the fabricated horns and a Langevin transducer. The horns are driven by the Langevin transducer.

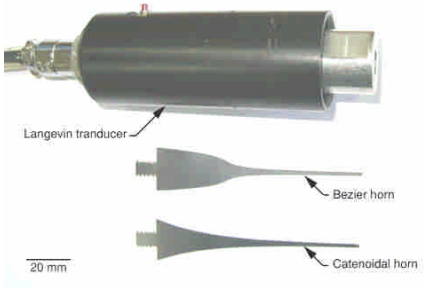

Fig. 11. Fabricated prototypes and a Langevin transducer.

Fig. 12(a) is a schematic of the experimental apparatus for measurement of the displacement/vibration of the horns. The horns are mounted on an optical table. AC voltages are applied to the Langevin transducer by an electronic circuit that works like a nearly ideal voltage source. The vibration amplitude of the horns is measured by a laser displacement sensor (LK-G5001, KEYENCE Corporation). The laser head LK-H020 is held by a micro manipulator. The measurement is recorded and analyzed by a KEYENCE software (LK-Navigator2).

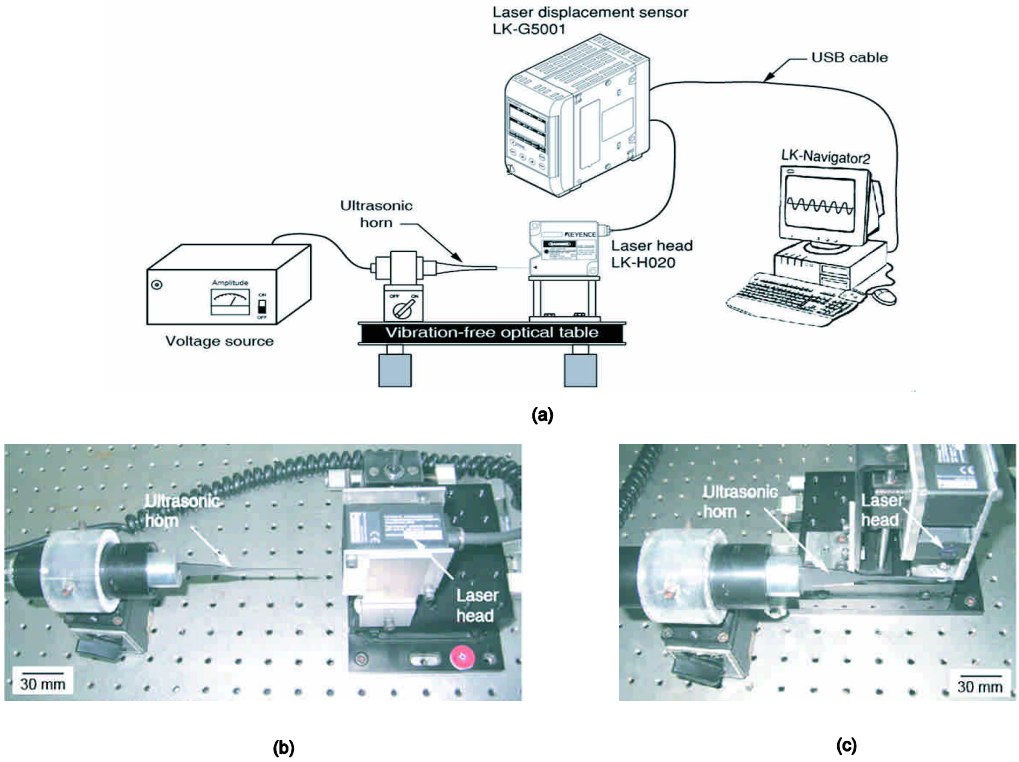

Fig. 12. (a) Schematic of the experimental apparatus. Experimental setup for measurement of (b) longitudinal and (c) flexural displacements.

In order to obtain the electrical power absorbed by the horns, a LCR meter (WK-4235, Wayne Kerr Electronics Ltd., UK) is used to measure the electrical input impedance of the horns. The test voltage of the LCR meter used in the experiments is 2.0 V_{rms}. Fig. 13(a) and (b) show the electrical input impedance and phase, respectively, of the Bézier and the catenoidal horn. As shown in Fig. 13(a), the measured working frequency of the Bézier horn is 28.2 kHz which is in a quite good agreement with that predicted in the analyses (see Fig. 6). For the catenoidal horn, the measured working frequency, 28.1 kHz, is nearly the same as that obtained by the finite element analysis. The experimental results indicate that the modulus of the impedance of the proposed horn is lower than that of the catenoidal horn at their respective working frequencies. Since the two horns are tested with the same voltage; being the electrical impedance at the working frequency of the proposed horn lower than that at the working frequency of the catenoidal horn, the Bézier horn is able to absorb a higher electrical power than the catenoidal horn.

When the system is driven in the operating mode and a combination resonance occurs, then a large amount of energy flows from the operating mode to the internal modes [24]. In the experiments, the system is excited close to its first longitudinal mode. It is assumed that the internal modes are not excited based on the finite element analyses. In order to verify this assumption, experiments are carried out to measure the flexural displacement/vibration of the horns driven in the longitudinal mode. Fig. 12(b) and (c) are photos of the experimental setup for measurement of the longitudinal and flexural displacements, respectively, of the horns driven in the longitudinal mode. The modal interactions should be investigated by using a 3D laser Doppler vibrometer. Due to the measurement equipments available, the laser displacement/vibration sensor is used for initial assessment of the modal interactions.

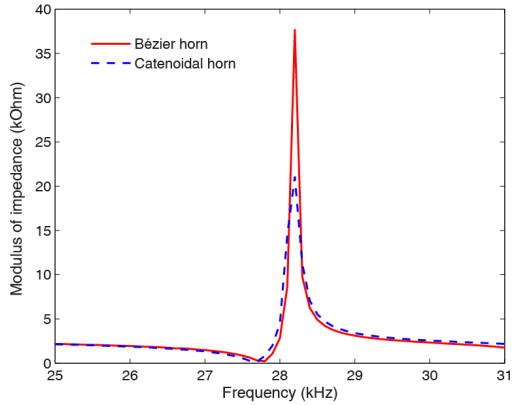

(a)

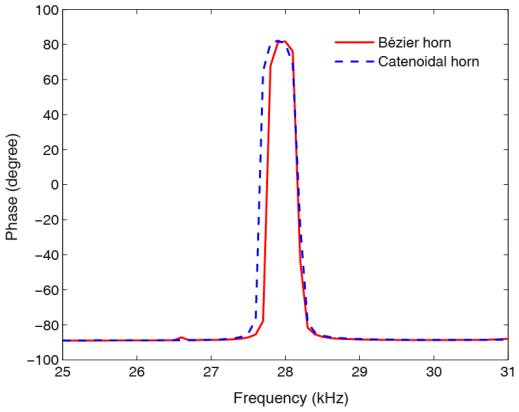

(b)

Fig. 13. Experimental results: (a) modulus of impendance and (b) phase.

Fig. 14(a) and (b) show the measured longitudinal and flexural vibration amplitude, respectively, of the horn tip when the horn is driven longitudinally. The responses of the longitudinal and flexural vibrations exhibited a single frequency response as shown in the figure. Some measurement noise of the flexural vibrations is also shown in Fig. 14(b). The noise can be attributed to the curved profile of the horn and the misalignment of the horn and the probe tip of the flexural vibration measurement setup.

Fig. 15 shows the measured vibration amplitude of the Bézier horn and the catenoidal horn as functions of the applied voltage at 28.2 kHz and 28.1 kHz, respectively. The vibration amplitudes of both horns increase as the driving voltage increases. The average displacement of the Bézier horn is approximately 30% greater than that of the catenoidal horn for the driving voltages considered. The simulation results listed in Table 1 shows that the Bézier horn has the displacement amplification 62% larger than the catenoidal horn while the experiment shows a nearly 30% of improvement. The manufacturing error and the misalignment due to assembly process may contribute to the discrepancy. It should be noted that high power ultrasonic components are prone to non-linear response with cubic softening or hardening. The discrepancy may also be attributed to the assumption that the finite element analyses carried out in this investigation are based on linear dynamic response.

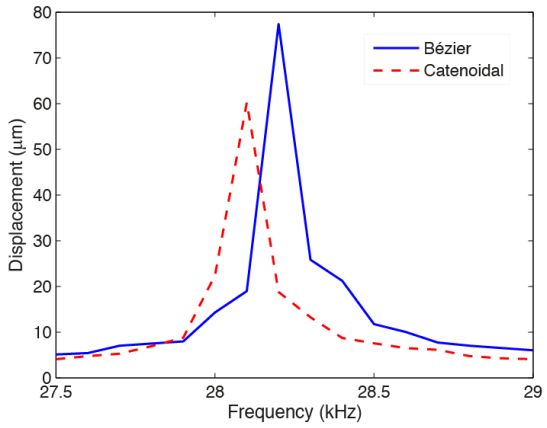

(a)

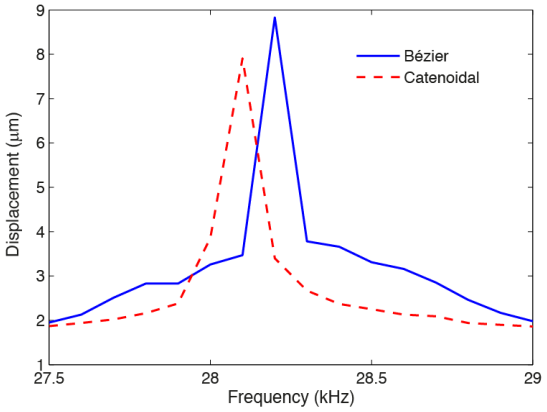

(b)

Fig. 14. Measured response of the (a) longitudinal and (b) flexural vibration amplitudes of the horn tip.

Fig. 16 is the harmonic response of the designed and fabricated Bézier horns near the working frequency, 28.2 kHz. The experimental working frequency of the Bézier horn, 28.2 kHz, is in a good agreement with that predicted by the finite element analyses without damping. When damping is considered in the finite element analysis, the simulated modal frequency should be lower than that without damping. It is suggested that the effects of damping on the first longitudinal modal frequency of the finite element model can be neglected due to the close agreement between the experiments and simulations for the purpose of the optimization design process of the proposed horn.

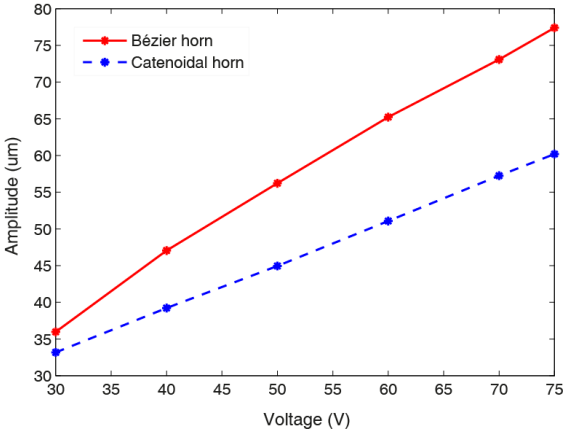

Fig. 15. Measured vibration amplitude of the horns as functions of the driving voltage.

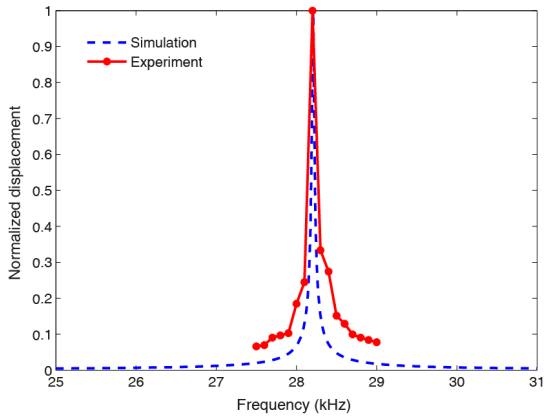

Fig. 16. Harmonic response of the designed and fabricated Bézier horns.

CONCLUSIONS

A planar horn with high displacement amplification is developed. The profile of the horn is a cubic Bézier curve. Its design procedure is based on a multi-objective optimization algorithm and finite element analyses. Based on the finite element analyses, maximum Mises stress of the proposed horn is much lower than that of the catenoidal horn. Prototypes of the horn have been fabricated and tested. Experimental comparison of the working frequency between the designed and fabricated Bézier horns validates the effectiveness of the optimization design method. The displacement amplification of the proposed horn is 30% higher than that of the traditional catenoidal horn with the same length and end surface widths.

REFERENCES

[1] R.R. Perron, The design and application of a reliable ultrasonic atomizer, IEEE Transactions on Sonics and Ultrasonics SU-14 (1967) 149–153.

[2] S. Charles, R. Williams, T.L. Poteat, Micromachined structures in ophthalmic microsurgery, Sensors and Actuators A21–A23 (1990) 263–266.

[3] L. Parrini, Design of advanced ultrasonic transducers for welding devices, IEEE Transactions on Ultrasonics, Ferroelectrics and Frequency Control 48 (2001) 1632–1639.

[4] S.W. Or, H.L.W. Chan, V.C. Lo, C.W. Yuen, Dynamics of an ultrasonic transducer used for wire bonding, IEEE Transactions on Ultrasonics, Ferroelectrics and Frequency Control 45 (1998) 1453–1460.

[5] L. Parrini, New technology for the design of advanced ultrasonic transducers for high-power applications, Ultrasonics 41 (2003) 261–269.

[6] J. Hu, K. Nakamura, S. Ueha, An analysis of a noncontact ultrasonic motor with an ultrasonically levitated rotor, Ultrasonics 35 (1997) 459–467.

[7] A. Iula, G. Caliano, A. Caronti, M. Pappalardo, A power transducer system for the ultrasonic lubrication of the continuous steel casting, IEEE Transactions on Evolutionary Computation 50 (2003) 1501–1508.

[8] A. Iula, S. Pallini, F. Fabrizi, R. Carotenuto, N. Lamberti, M. Pappalardo, A high frequency ultrasonic bistoury designed to reduce friction trauma in cystectomy operations, in: Proceedings of 2001 IEEE Ultrasonics Symposium, 2001, pp. 1331–1334.

[9] C.-H. Lee and A. Lal, Silicon ultrasonic horns for thin film accelerated stress testing, in: Proceedings of 2001 IEEE Ultrasonics Symposium, 2001, pp. 867– 870.

[10] E. Eisner, Design of sonic amplitude transformers for high magnification, The Journal of the Acoustical Society of America 35 (1963) 1367–1377.

[11] A. Bangviwat, H.K. Ponnekanti, R.D. Finch, Optimizing the performance of piezoelectric drivers that use stepped horns, The Journal of the Acoustical Society of America 90 (1991) 1223–1229.

[12] D. Sindayihebura, L. Bolle, Theoretical and experimental study of transducers aimed at low-frequency ultrasonic atomization of liquids, The Journal of the Acoustical Society of America 103 (1998) 1442–1448.

[13] B.N. Nagarkar, R.D. Finch, Sinusoidal horns, The Journal of the Acoustical Society of America 50 (1971) 23–31.

[14] K.F. Graff, Wave Motion in Elastic Solids, The Clarendon Press, Oxford, 1975.

[15] V. Salmon, A new family of horns, The Journal of the Acoustical Society of America 17 (1946) 212–218.

[16] S. Sherrit, S.A. Askins, M. Gradziol, B.P. Dolgin, X. Bao, Z. Chang, Y. Bar-Cohen, Novel horn designs for ultrasonic/sonic cleaning welding, soldering, cutting and drilling, in: Proceedings of the SPIE Smart Structures Conference, vol. 4701, Paper No. 34, San Diego, CA, 2002.

[17] A. Iula, L. Parenti, F. Fabrizi, M. Pappalardo, A high displacement ultrasonic actuator based on a flexural mechanical amplifier, Sensors and Actuators A 125 (2006) 118–123.
[18] O.V. Abramov, High-intensity Ultrasonics: Theory and Industrial Applications, Gordon and Breach Science Publishers, The Netherlands, 1998.
[19] D.F. Rogers, J.A. Adams, Mathematical Elements for Computer Graphics, second ed., McGRAW-Hill, New York, 1990.
[20] J. Woo, Y. Roh, K. Kang, S. Lee, Design and construction of an acoustic horn for high power ultrasonic transducers, in: Proceedings of 2006 IEEE Ultrasonics Symposium, 2006, pp. 1922–1925.
[21] B. Fu, T. Hemsel, J. Wallaschek, Piezoelectric transducer design via multiobjective optimization, Ultrasonics 44 (2006) e747–e752.
[22] K. Deb, A. Pratap, S. Agarwal, T. Meyarivan, A fast and elitist multiobjective genetic algorithm: NSGA-II, IEEE Transactions on Evolutionary Computation 6 (2002) 182–197.
[23] D.E. Goldberg, Genetic Algorithms in Search, Optimization & Machine Learning, Addison Wesley Publishing Company, Inc., MA, 1989.
[24] A. Cardoni, M. Lucas, M. Cartmell, F. Lim, A novel multiple blade ultrasonic cutting device, Ultrasonics 42 (2004) 69–74.